PAPER

Check for updates

Preparation of perovskite CsPb(Br$_x$I$_{1−x}$)$_3$ quantum dots at room temperature

Ying Li,[a] Jun Qian, *[ab] Di Zhao[a] and Rong Song[a]

Here, we propose a method for preparing red perovskite CsPb(Br$_x$I$_{1−x}$)$_3$ quantum dots (QDs) at room temperature. The PL emission peak of the QDs is close to 650 nm, and the full width at half maximum reaches 61 nm. The red CsPb(Br$_x$I$_{1−x}$)$_3$ QDs with higher water stability are obtained successfully at room temperature by adjusting the proportion of halogen elements and incorporating polystyrene. At the same time, the red QDs are combined with a blue light-emitting diode to prepare a white light-emitting device (WLED). Compared with the WLED based on the Ce-doped Yttrium Aluminum Garnet (YAG:Ce) phosphor alone, the new WLED based on QDs exhibits a reduced correlated color temperature of 2976 K, while achieving a lumen efficiency of 55.3 lm W$^{−1}$, which provides a feasible solution for future research on light-emitting diodes (LEDs).

1. Introduction

In the late 1970s, the first preparation and application of organic–inorganic hybrid perovskites (such as $CH_3NH_3SnX_3$ and $CH_3NH_3PbX_3$) attracted the attention of a large number of early scientists.[1] As is well-known, both ion exchange and doping affect the electronic band structure.[2–4] Therefore, depending on the combination of these anions and cations, perovskite materials can exhibit different characteristics, such as superconductivity, piezoelectric, insulating, anti-ferromagnetic, and photoelectric properties.[5–8] So far, these nanomaterials have been demonstrated as promising building blocks for solar cells, flexible sensors, and silicon-based photonics, and they are even expected to be used in biological detection and electrically driven lasers.[9–12] As a result, these materials have been developed rapidly over the past decade.

With the gradual deepening of research, some defects of organic–inorganic hybrid perovskites have been gradually exposed, especially in the case of halogen-containing iodine-based perovskites. Illumination degrades the perovskite to produce iodine vapor, and iodine vapor accelerates the decomposition of the perovskite, so the perovskite is extremely unstable.[13–19] In 2015, the Kovalenko team prepared inorganic halide perovskite QDs successfully according to the high-temperature thermal injection method.[20] They replaced the A-site organic cation with a more stable inorganic cation (Cs^+). These all-inorganic perovskite QDs have achieved not only higher luminous efficiency, but also improved stability

compared to the organic–inorganic hybrid perovskite QDs. Subsequently, a lot of reports about the preparation, application, and performance of inorganic halide perovskite QDs have been reported,[21] and this has become a research hotspot of perovskite materials.

The conventional methods for preparing all-inorganic perovskites include thermal injection, supersaturated recrystallization, chemical vapor deposition and so on.[22] In the thermal injection method, the growth of perovskite crystals can be controlled by changing the crystal growth direction and changing the concentration of the reactants, which controls the potential energy of monomers in the chemical reaction.[23–26] The temperature is difficult to control strictly because of the injection of the precursor solution. So, it is difficult to ensure that the production products are the same in mass production.[27,28] Also, the synthesis process is complicated, and it is necessary to maintain the high temperature of the precursor solution and the nitrogen gas environment to isolate oxygen during the experiment. These disadvantages limit the large-scale application of thermal injection methods in commercial preparation. Compared with the hot injection method, the supersaturation recrystallization method (SRM) has a fast reaction process, a short cycle, and a relatively low preparation temperature requirement (about 100 °C).[29–32] Although this method for preparing $CsPbBr_3$ is relatively mature, there are still many problems (such as controlling crystal growth, and mass production of red perovskite) in the method when changing the halogen composition.[33] Doped heavy metals and composite materials[34,35] have been used to prepare red perovskite due to the increasing demand for stable and highly fluorescent materials. Increasingly, the above preparation method obviously cannot meet the requirements for mass production of

[a]*School of Printing and Packaging, Wuhan University, 129 Luoyu St. Hongshan, Wuhan, China. E-mail: qianjungreat@whu.edu.cn*

[b]*Lab of Green Platemaking and Standardization for Flexographic Printing, Shanghai Publishing and Printing College, Shanghai, 200093, China*

materials. Until now, a simplified preparation method for red perovskite is still a key research topic for scientists.

In 2018, Helder Scapin Anizelli and his team prepared a $CH_3NH_3Pb(Br_xI_{1-x})_3$ inorganic halide perovskite QD film successfully by spin coating at 70 °C.[36] However, the all-inorganic perovskite is easily quenched by water, which limits its daily application to a certain extent. Polystyrene (PS) has a refractive index of about 1.5 and has good transparency. At the same time, the presence of the benzene ring makes it have better barrier properties, and its low cost, good flexibility, and colorless characteristics[37–40] meet the performance requirements of quantum dots/polymer films and improve the stability of composite materials. In this case, our group proposed a low-cost, improved solution method that red $CsPb(I_{1-x}Br_x)_3$ perovskite can be prepared in large quantities at room temperature with excellent water stability.

In this paper, we focused on the improvement of the preparation method of $CsPbX_3$ QDs and prepared the perovskite in a convenient and environmentally friendly way. At the same time, the improved method was used to verify the color adjustment mechanism of $CsPbX_3$ QDs. Since the preparation of red $CsPb(Br_xI_{1-x})_3$ QDs was extremely unstable, a set of improved methods was developed for this problem. This preparation method is different from the spin coating method and the general reprecipitation method: the red perovskite solution/film can be prepared on a large scale in a non-protective atmosphere at room temperature, and the water stability of QDs is greatly improved. This method simplifies the preparation conditions and expands the application range of red $CsPb(Br_xI_{1-x})_3$ QDs. For example, liquid perovskite can be applied to LEDs of various shapes or printed with different fluorescent patterns, and so on. We prepared a white light-emitting device by using $CsPb(Br_xI_{1-x})_3$ QDs and a Ce-doped Yttrium Aluminum Garnet (YAG:Ce) phosphor combined with blue light. After testing, it can be seen that the color coordinates are adjusted to a warmer place (0.3603, 0.2384), which is more comfortable to the human body, and the correlated color temperature is also lowered to 2976 K. We also calculated the lumen efficiency. The result is $\Phi/(U \times I) = 6.8/(4.1 \times 0.03) = 55.3$ lm W^{-1}. This value proves that the LED prepared in this work has better photoelectric conversion efficiency and higher LED brightness.

2. Experimental section

2.1 Materials

The materials cesium bromide (CsBr), lead(II) iodide (PbI_2), lead(II) bromide ($PbBr_2$), polymethyl methacrylate (PMMA), Ce-doped yttrium aluminum garnet (YAG:Ce) phosphor, and polystyrene (PS) were all purchased from Aladdin. Dimethylformamide (DMF), trichloromethane (MSDS), and ethyl acetate (EAC) were furnished by the Sinopharm Group.

2.2 Preparation of red $CsPb(Br_xI_{1-x})_3$ QDs

Red $CsPb(Br_xI_{1-x})_3$ QDs were prepared by SRM at room-temperature. First of all, 0.2 mmol PbI_2 and 0.2 mmol CsBr

were mixed with 5 mL of DMF and 0.02 g of PMMA (the green QDs were prepared from 0.2 mmol $PbBr_2$ and 0.2 mmol CsBr, and the yellow QDs were prepared from 0.1 mmol $PbBr_2$, 0.1 mmol PbI_2 and 0.2 mmol CsBr). The mixture was placed in a constant temperature magnetic stirrer and stirred vigorously at 20 °C until the precipitate in the mixed solution was dissolved. Then, 12 mL of ethyl acetate was added into the solution and an orange turbid called liquid A was formed. This solution was quickly taken out from the constant temperature water bath and transferred to a 4 mL centrifuge tube and centrifuged at 8500 rpm for 2 minutes in a centrifuge. The supernatant was separated, and 1 mL of ethyl acetate was slowly added to each centrifuge tube. The $CsPb(Br_xI_{1-x})_3$ QDs, which excite red fluorescence, can be obtained by separating the liquid and the precipitate after shaking the centrifuge tube. Besides, a set of reaction temperature gradients were set at low temperature with the remaining variables unchanged, and we set four control experiments at 20 °C to 50 °C (temperature gradient experiments were performed only in the preparation of red QDs).

2.3 Stability improvement of $CsPb(Br_xI_{1-x})_3$ QDs

Stable composite QDs were prepared at room temperature (20 °C). 3 g of PS and 10 mL of MSDS were mixed in a 50 mL flask at 45 °C, and a PS and MSDS mixture was obtained. The PS solution and the QD solution were mixed in different proportions to obtain a series of QD/PS composite solutions in different proportions. The PET film was put on a spin coater, and the vacuum pump was turned on to draw a vacuum so that the PET film was adsorbed on the surface of the spin coater on the stage. It was spin-coated into a film at a speed of 3000 rpm for 30 seconds for the next characterization.

2.4 Calculation of the quantum yield

The PLQY of the $CsPb(Br_xI_{1-x})_3$ QDs was calculated using rhodamine B as a reference. The excitation wavelength was 375 nm, and the PLQY of rhodamine B at the excitation wavelength of 375 nm was 97%. The absorbances of the QD/PS composite solutions and the rhodamine B solution were both less than 0.05. The PLQY calculation formula is as follows:

$$Y_u = Y_s \times \frac{F_u}{F_s} \times \frac{A_s}{A_u} \times \frac{\eta_u}{\eta_s}$$

Here, u stands for the sample to be tested, s is a reference, Y is the quantum yield, F stands for the integrated area of the emission spectrum curve, and η represents the refractive index of the solvent. The solvent of the QD solution in this experiment was n-hexane ($\eta = 1.38$), and the solvent of rhodamine B was ethanol ($\eta = 1.36$).

2.5 Preparation of LEDs

PMMA was selected as a dispersant and solidifying agent of the fluorescent material to promote the fluorescent material forming a coating on the LED and quickly solidifying. The amount of YAG:Ce phosphor and PMMA (melt with a small amount of EAC in advance for use) should be fully mixed. Then, a microsyringe was used to inject the mixture into the surface of the blue LED,

and press it several times as weighing paper. The LED was seasoned by a hot hair dryer for about 10 s. This LED is a blank control. In addition, the QD/PS mixed liquid in part 2.3 was mixed with YAG:Ce phosphor (the same amount as the blank control) and PMMA. Similarly, the mixture was dropped onto the surface of the blue LED and heated by a hairdryer after pressing.

2.6 Characterization

The absorption spectra were recorded at room temperature using a UV-Vis spectrophotometer (CARY 5000, Varian, America). The PL spectrum was measured at room temperature using an F-4600 fluorescence spectrometer (5J2-0004, Japan). Transmission electron microscopy (TEM) was measured by an electron microscope (JEM-2100, Japan). The X-ray diffraction pattern (XRD) was measured using a diffractometer with Cu Kα ($\lambda = 0.15418$ nm) radiation (XPert Pro, PANalyco, Netherlands). The EL spectra were collected by using an HP DC voltage stabilized current power, a fiber integration sphere, and an HPS-2000 spectrometer in air and at room temperature.

3. Results and discussion

3.1 Phase analysis of CsPb(Br$_x$I$_{1-x}$)$_3$ QDs

The three major XRD diffraction peaks are moved by adjusting the molar ratio of Br/I (the preparation temperature is 20 °C), as shown in Fig. 1(a). As the content of the I element increases, the diffraction peaks of the perovskite crystal tend to a low angular offset. Besides, different proportions of CsPb(Br$_x$I$_{1-x}$)$_3$ QDs also exhibit a cubic phase at low temperatures. The movement of the position of the main peaks is regular, so the substitution of anions in the perovskite structure does not change its phase
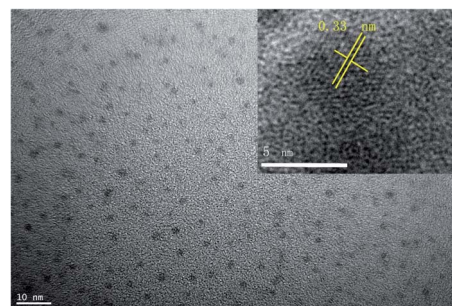
Fig. 2   TEM images of red-light CsPb(Br$_x$I$_{1-x}$)$_3$ perovskite crystals.

significantly. We can explain that by the Bragg equation $2d \sin \theta = n\lambda$. The interplanar spacing d becomes larger and the θ becomes smaller when the incident light wavelength λ is constant. Therefore, when I$^-$ is used instead of Br$^-$ with a larger ionic radius, the d becomes larger and the diffraction peak moves toward a low angle. Meanwhile, there are many hetero peaks in the three XRD patterns of CsPb(Br$_x$I$_{1-x}$)$_3$ QDs, which show that the incorporation of I$^-$ reduces the crystallization. At the same time, there may be other chemical reactions.

To further understand the series of substances generated during the preparation of red CsPb(Br$_x$I$_{1-x}$)$_3$, the XRD diffraction pattern was obtained for the precipitates remaining after separating the luminescent perovskite crystals in Section 2.2. As shown in Fig. 1(b), the pattern was analyzed using the Jade software with the PDF standard card, and the peaks of the pattern were found to correspond to the standard PDF number of other inorganic substances, such as Cs (42-1246), I$_2$ (43-0304), and CsIBr$_2$ (32-0223). The precipitate contains inorganic substances such as Cs, I$_2$, and CsIBr$_2$, and the composition is relatively complicated. During the reaction, other chemical reactions are generated with useless inorganic substances. A large amount of non-luminescent solid remains during the preparation of red QDs. The element utilization ratio of the perovskite is lower than that of the preparation of CsPbBr$_3$.

The red CsPb(Br$_x$I$_{1-x}$)$_3$ perovskite crystal prepared at 20 °C was tested by TEM. As shown in Fig. 2, the QDs are uniformly dispersed in the solvent, and the size of each quantum dot is about 3 nm. The inset shows that by continuing to magnify the resolution, the growth trend of the lattice fringes and composite
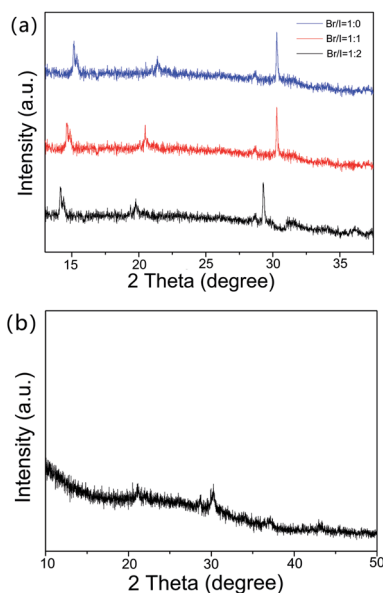

Fig. 1   (a) XRD pattern of perovskites prepared with different Br/I ratios (the molar ratios of Br/I are 1 : 0, 1 : 1 and 1 : 2, respectively); (b) XRD pattern of the precipitate without luminescence formed during preparation.
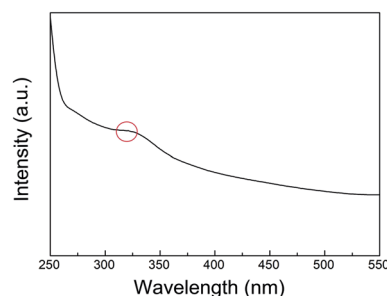

Fig. 3   Absorption spectra of red-light CsPb(Br$_x$I$_{1-x}$)$_3$ perovskite QDs prepared at 20 °C.

perovskite QDs growing on the (110) crystal plane can be observed.

3.2 Optical properties of CsPb(Br$_x$I$_{1-x}$)$_3$ QDs

Since red QDs prepared at 20 °C are extremely unstable, they are suspected to be related to temperature. First of all, the absorption spectrum of the QDs at a preparation temperature of 20 °C was obtained. As shown in Fig. 3, we can see that the absorption peak is at about 325 nm.

To explore the influence of different temperatures on the luminescence of the red QDs at medium and low temperatures, the red CsPb(I$_{1-x}$Br$_x$)$_3$ prepared under four temperature gradients are set. The red fluorescence excited by the samples did not differ greatly under the excitation of UV light of about 325 nm (inset in Fig. 4(a)), so the four groups of samples were tested by PL spectroscopy.

The PL spectra shown in Fig. 4(a) of the red CsPb(I$_{1-x}$Br$_x$)$_3$ perovskites prepared at different temperatures under the low-temperature conditions are similar. The PL wavelengths at 40 °C and 50 °C almost overlap (about 655 nm), indicating that the preparation temperature has little effect on the luminescence performance of the perovskite in the low-temperature range. However, the red QDs prepared by the improved solution method are completely quenched after a few days without any treatment, as shown in Fig. 4(b), which greatly limits their large-scale application.

3.3 Optical properties of stable coated CsPb(Br$_x$I$_{1-x}$)$_3$ QDs

Combining the above experiments and analysis, taking 20 °C as the preparation temperature as an example, the red QDs were subjected to stability coating treatment. PS is often easily soluble in strongly polar solvents such as DMF, while CsPb(Br$_x$I$_{1-x}$)$_3$ QDs can only be dissolved in non-polar solvents, such as n-hexane, toluene, and MSDS, or weakly polar solutions. Therefore, we chose to dissolve the QDs with a weak polarity solution based on the principle of similar compatibility.

The PL emission spectra of the QDs/PS luminescent films synthesized at different ratios at 20 °C are shown in Fig. 5. It can be observed that the position of the PL peak is not much different from that of the original QD film without coating. It is still near 650 nm, and the half-width of the emission peak is
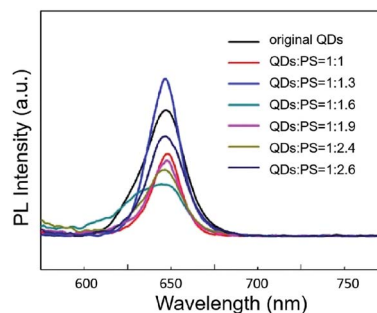
Fig. 5 PL emission spectra of the QD/PS luminescent film synthesized at different ratios at 20 °C.

narrowed. Furthermore, the position of the emission peak is not affected by the polymer concentration. Besides, when PS is added, the fluorescence intensity of the composite material is reduced, because organic matter hinders part of the light transmission. When the ratio of QDs to PS is 1 : 1.3, the emission peak is the highest, and the prepared film has the best luminescence performance. The reason for this phenomenon is that organic polymers (PS) have greater steric hindrance, which can effectively coat QDs and better avoid the reaction between the QDs and air and oxygen. At the same time, some molecular bonds in PS can combine with some non-radiative defects in the QDs to protect their fluorescence characteristics. However, too much PS will hinder light transmission, thereby reducing the fluorescence intensity of the QDs.

Take the three PS composite ratios with the best optical performance as an example to verify the uniformity of the QD/PS composites. Shown in Fig. 6 is a picture of a composite
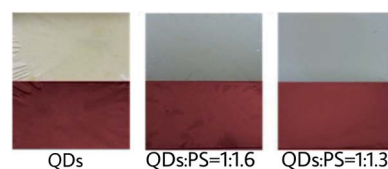
Fig. 6 CsPb(Br$_x$I$_{1-x}$)$_3$/PS films prepared in different proportions under sunlight (top) and UV light (bottom).

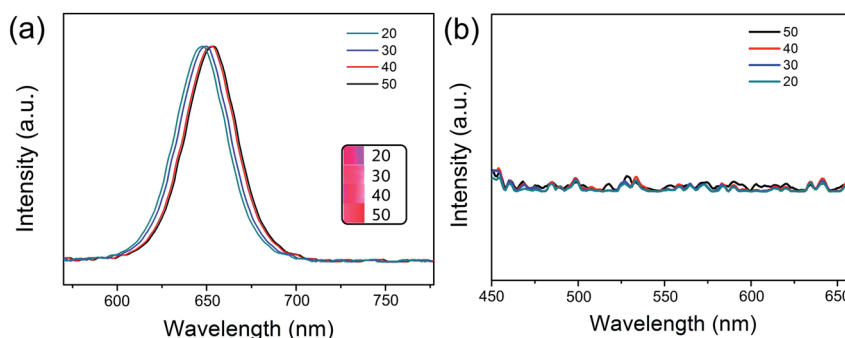**Fig. 4** (a) and (b) PL emission spectra of red-light CsPb(Br$_x$I$_{1-x}$)$_3$ prepared at different temperatures and placed in a normal environment for 2 days (curve unit: °C) and (inset in (a)) QDs prepared at 20 °C, 30 °C, 40 °C and 50 °C reaction temperatures (under 325 nm UV light).

film prepared with different volume ratios of QDs and PS under sunlight and ultraviolet light. We can see that the uniformity and smoothness of the film are significantly improved with PS. When the ratio of QDs to PS is 1 : 1.3, the surface uniformity of the sample is the best. When the PS content continues to increase, the sample becomes uneven again. Although the red light is excited, the film's surface uniformity is poor, and there are many clusters on the surface of the film. The large difference in polarity between the MSDS and DMF solutions and the different hydrophilicity results in different internal stresses, which will affect the uniformity and color of the film.

To explore whether the different ratios of QDs and PS will affect the stability of the quantum dot light-emitting film, we immerse six samples of QDs/PS composite films manufactured in different ratios in water for 30 min, and test the emission spectra before and after immersion. As shown in Fig. 7, when the ratio of $CsPb(Br_xI_{1-x})_3$ to PS is 1 : 1.3, the PL spectra change the least and the film has the best stability. We calculated the spectral area and the fluorescence intensity change of the composite film: when the ratio of QDs to PS is 1 : 1.3, the fluorescence intensity after immersion is 86% of that before immersion. Based on the conclusions in the figure, when the ratio is 1 : 1.3, the luminous intensity and stability of the film are the best. Therefore, we will adopt the QD : PS = 1 : 1.3 ratio for the next experiment.

To evaluate the stability of the composite film, a set of uncoated pure $CsPb(I_{1-x}Br_x)_3$ films were designed for comparison. Fig. 8 shows the relative intensity change of the two groups of luminescent films in 80 minutes. The fluorescence intensity was measured at intervals of 8 minutes. It can be seen that the fluorescence intensity of the uncoated pure QD film decreases rapidly within 8 minutes, and the fluorescence characteristics are completely lost in about 20 minutes. In contrast, the fluorescence intensity of the PS-coated QD film is not significantly
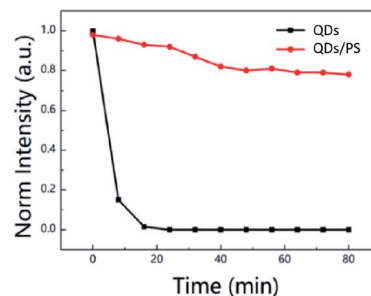

Fig. 8 The fluorescence intensity changes of the two groups of films after immersing in water for 80 min.

reduced after immersion in water, and it can still maintain about 80% of the fluorescence after being immersed in water for 80 minutes. Therefore, we can conclude that the PS-coated QDs can maintain high fluorescence intensity in water, which greatly improves the stability of $CsPb(Br_xI_{1-x})_3$ in water.

Based on the comparison of the PL spectra of the polymer composite films, when the ratio of QDs to PS is 1 : 1.3, the QDs/PS composite has a narrow peak width at half height (FWHM) of the emission peak, and its PLQY is 57%. The composite material also has high uniformity and water stability. We determined that the composite material has relatively better light-emitting performance, so we chose this material to prepare LED devices.

3.4 Photoelectronic properties of QD-converted LEDs

The electroluminescence (EL) spectrum and color coordinates of the conventional white light-emitting device prepared by a YAG:Ce phosphor are shown in Fig. 9.

In this test, the device lacks long-wavelength components, and the correlated color temperature is displayed as 3829 K,
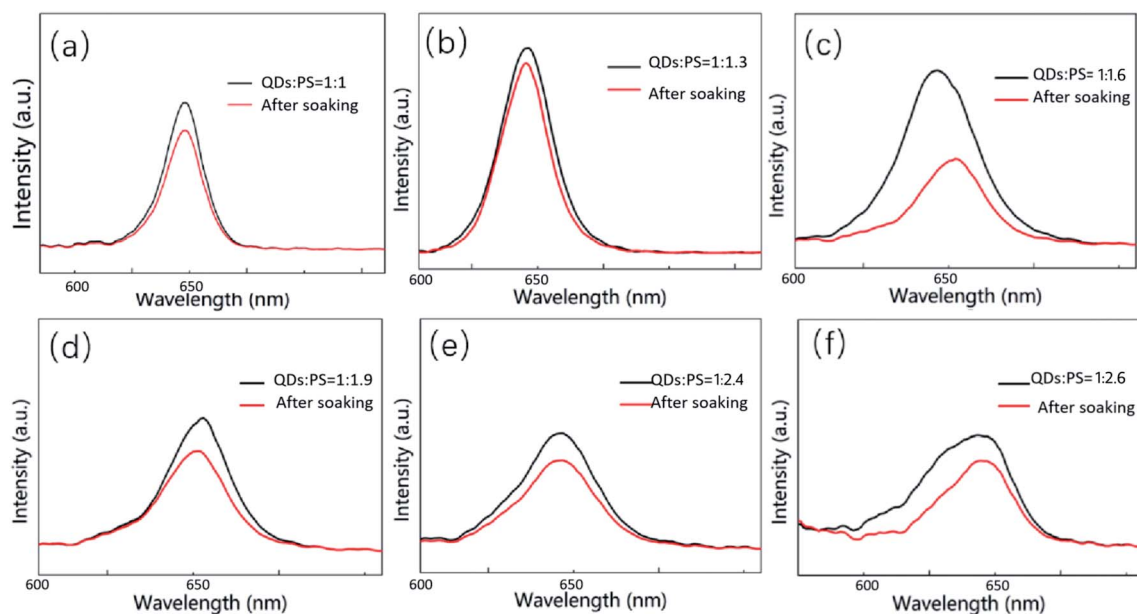

Fig. 7 PL spectra of CsPbBr₃/PS films with different proportions before and after immersion in water.
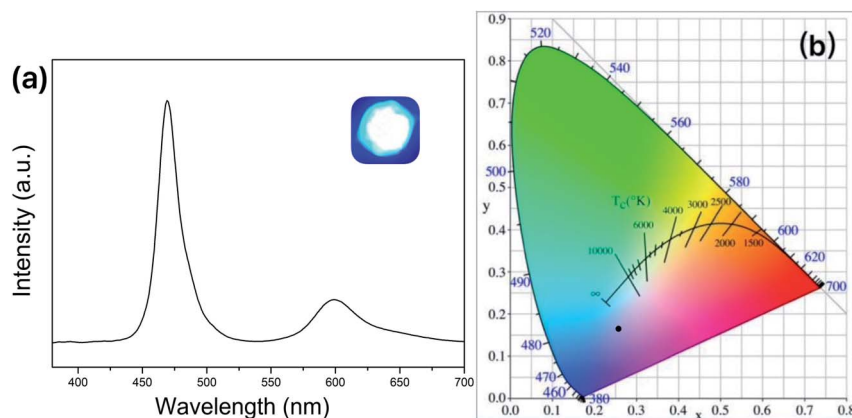
Fig. 9 YAG:Ce phosphor composite on a blue LED: (a) emission spectrum; (b) corresponding CIE color coordinates.
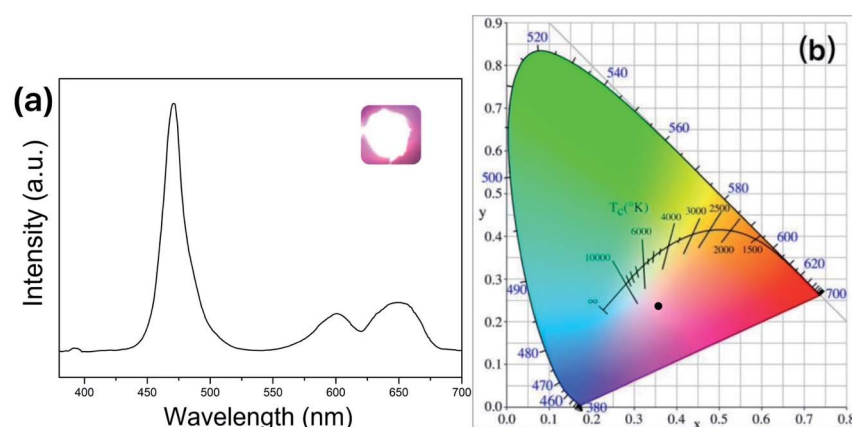

Fig. 10 LED test with the red QDs and YAG:Ce phosphor composite: (a) emission spectrum; (b) CIE color coordinates.

which is relatively high. This LED emits cold light and is not suitable for daily lighting. To improve the situation, the composite addition of red $CsPb(Br_xI_{1-x})_3$ prepared by the improved solution method can effectively improve the performance of the device. As shown in Fig. 10, the LED is prepared by coating the red QD composite with the emission wavelength of 650 nm.

As shown in Fig. 10(b), the coordinates of the light emitted by the LED are warmer (0.3603, 0.2384), and the correlated color temperature is also reduced to 2976 K. The LED can be considered to emit warm white light. The lumen efficiency is as follows:

$$\Phi/(U \times I) = 6.8/(4.1 \times 0.03) = 55.3 \text{ lm W}^{-1}$$

Here, Φ is the luminous flux, and U and I are the excitation voltage and current of the LED, respectively. The above data can be directly obtained by the fiber integration sphere. The final calculated lumen efficiency proves that the LED prepared in this part has better photoelectric conversion efficiency and higher LED brightness, and there is great value of $CsPb(Br_xI_{1-x})_3$ QDs in composite applications of LEDs.

4. Conclusions

In summary, red $CsPb(Br_xI_{1-x})_3$ QDs can be synthesized at low temperature. They were prepared by the modified solution method at 20, 30, 40 and 50 °C, and the change of the preparation temperature has no great influence on the change of the excitation light wavelength of the quantum dots. Organic matter coating can effectively improve the stability of QDs and form stable solid-state QDs at room temperature. PL spectrum analysis shows that the water stability and uniformity of the QDs are slightly improved through the coating of PS (best ratio: QDs : PS = 1 : 1.3). The correlated color temperature of the LED prepared by stabilizing the QDs can be reduced to 2976 K, and the compound effect of the quantum dots is more obvious. At the same time, by calculating the lumen efficiency (55.3 lm W^{-1}), the LED has strong brightness and high photoelectric conversion efficiency. This provides the possibility for mass production of red QDs, and the stability of the red QD solution also provides the possibility for full-spectrum printable perovskite inks. We expect QDs to provide a new idea for the commercial production of LEDs and back electrodes in the future.

Conflicts of interest

There are no conflicts to declare.

Acknowledgements

References

1 D. Weber, $CH_3NH_3SnBr_xI_{3-x}$(x=0-3), ein Sn(II)-System mit kubischer Perowskit Struktur/$CH_3NH_3SnBr_xI_{3-x}$(x=0-3), a Sn(II)-System with Cubic Perovskite Structure, *Z. Naturforsch. B Chem. Sci.*, 2014, **33**, 862–865.

2 S. S. A. Al-Abbas, M. K. Muhsin and H. R. Jappor, Two-dimensional GaTe monolayer as a potential gas sensor for SO_2 and NO_2 with discriminate optical properties, *Superlattices Microstruct.*, 2019, **135**, 106245.

3 M. M. Obeid, C. Stampfl, A. Bafekry, *et al.*, First-principles investigation of nonmetal doped single-layer BiOBr as a potential photocatalyst with a low recombination rate, *Phys. Chem. Chem. Phys.*, 2020, **22**(27), 15354–15364.

4 H. R. Jappor, Z. A. Saleh and M. A. Abdulsattar, Simulation of Electronic Structure of Aluminum Phosphide Nanocrystals Using Ab Initio Large Unit Cell Method, *Adv. Mater. Sci. Eng.*, 2012, 180679.

5 H. Liu, Y. Tan, M. Cao, *et al.*, Fabricating $CsPbX_3$-Based Type I and Type II Heterostructures by Tuning the Halide Composition of Janus $CsPbX_3/ZrO_2$ Nanocrystals, *ACS Nano*, 2019, **13**(5), 5366–5374.

6 J. Dai, J. Xi, L. Li, *et al.*, Charge Transport between Coupling Colloidal Perovskite Quantum Dots Assisted by Functional Conjugated Ligands, *Angew. Chem., Int. Ed.*, 2018, **57**, 5754–5758.

7 H. Wang, N. Sui, X. Bai, *et al.*, Emission Recovery and Stability Enhancement of Inorganic Perovskite Quantum Dots, *J. Phys. Chem. Lett.*, 2018, **9**, 4166–4173.

8 Y. Wang, M. Zhi, Y. Q. Chang, *et al.*, Stable, Ultralow Threshold Amplified Spontaneous Emission from $CsPbBr_3$ Nanoparticles Exhibiting Trion Gain, *Nano Lett.*, 2018, **18**, 4976–4984.

9 Q. Yang, C. Y. Li, J. H. Li, *et al.*, Multi-emitting fluorescence sensor of MnO_2-OPD-QD for the multiplex and visual detection of ascorbic acid and alkaline phosphatase, *J. Mater. Chem. C*, 2020, **8**(16), 5554–5561.

10 J. L. Yu, X. Y. Wang, Q. Kang, *et al.*, One-pot synthesis of a quantum dot-based molecular imprinting nanosensor for highly selective and sensitive fluorescence detection of 4-nitrophenol in environmental waters, *Environ. Sci.: Nano*, 2017, **4**(2), 493–502.

11 Q. Yang, J. H. Li, X. Y. Wang, *et al.*, Ternary Emission of a Blue-, Green-, and Red-Based Molecular Imprinting Fluorescence Sensor for the Multiplexed and Visual Detection of Bovine Hemoglobin, *Anal. Chem.*, 2019, **91**(10), 6561–6568.

12 D. H. Nguyen, J. Y. Sun, C. Y. Lo, *et al.*, Ultralow-Threshold Continuous-Wave Room-Temperature Crystal-Fiber/Nano perovskite Hybrid Lasers for All-Optical Photonic Integration, *Adv. Mater.*, 2021, **33**(12), 2006819.

13 P. Lu, M. Lu, H. Wang, *et al.*, Metal Halide Perovskite Nanocrystals and Their Applications in Optoelectronic Devices, *InfoMat*, 2019, **1**(4), 430–459.

14 Y. Song, S. Choi, J. Yoo, B. Kang and E. Ji, Design of long-term stable red-emitting $CsPb(Br_{0.4}, I_{0.6})_3$ perovskite, *Chem. Eng. J.*, 2017, **313**, 461–465.

15 Q. Sun and W. J. Yin, Thermodynamic Stability Trend of Cubic Perovskites, *J. Am. Chem. Soc.*, 2017, **139**(42), 14905–14908.

16 G. Divitini, S. Cacovich, *et al.*, Study on the stability of organic-inorganic perovskite solar cell materials based on first principle, *Mol. Phys.*, 2019, **1**, 1–11.

17 D. Bryant, N. Aristidou, S. Pont, S. M. Irene, C. Thana, W. Scot, R. D. James and A. H. Saif, Light and oxygen induced degradation limits the operational stability of methylammonium lead triiodide perovskite solar cells, *Energy Environ. Sci.*, 2016, **9**, 1655–1661.

18 H. F. Yuan, E. Debroye, K. Janssen, H. Naiki, C. Steuwe, G. Lu, M. Moris, E. Orgiu, U. Hiroshi, D. S. Frans, S. Paolo, H. Johan and R. Maarten, J. Degradation of Methylammonium Lead Iodide Perovskite Structures through Light and Electron Beam Driven Ion Migration, *J. Phys. Chem. Lett.*, 2016, **7**, 561–566.

19 W. Lv, L. Li, M. Xu, *et al.*, Improving the Stability of Metal Halide Perovskite Quantum Dots by Encapsulation, *Adv. Mater.*, 2019, **31**(28), 1900682.

20 D. Wei, T. Wang, J. Ji, S. M. C. Li, P. Cui, Y. Y. Li, G. Y. Li, M. M. Joseph and S. Dandan, Photo-induced degradation of lead halide perovskite solar cells caused by the hole transport layer/metal electrode interface, *J. Mater. Chem. A*, 2016, **4**, 1991–1998.

21 F. Zhang, Z. Shi, S. Li, *et al.*, Synergetic Effect of the Surfactant and Silica Coating on the Enhanced Emission and Stability of Perovskite Quantum Dots for Anticounterfeiting, *ACS Appl. Mater. Interfaces*, 2019, **11**(31), 28013–28022.

22 Y. He, J. Guo, Y. Zhu, X. Feng, H. Peng, W. Wang, H. He and H. Liu, Highly pure yellow light emission of perovskite $CsPb(Br_xI_{1-x})_3$ quantum dots and their application for yellow light-emitting diodes, *Opt. Mater.*, 2018, **80**, 1–6.

23 P. Guo, M. Hossain, X. Shen, H. Sun, W. Yang, C. Liu, C. Ho, C. Kwok, S. Tsang and Y. Luo, Room-Temperature Red-Green-Blue Whispering-Gallery Mode Lasing and White-Light Emission from Cesium Lead Halide Perovskite ($CsPbX_3$, X = Cl, Br, I) Microstructures, *Adv. Opt. Mater.*, 2018, **6**, 201700993.

24 A. Pan, B. He, X. Fan, *et al.*, Insight into the Ligand-Mediated Synthesis of Colloidal $CsPbBr_3$ Perovskite Nanocrystals: The Role of Organic Acid, Base, and Cesium Precursors, *ACS Nano*, 2016, **10**, 7943–7954.

25 M. C. Weidman, M. Seita, S. D. Stranks, *et al.*, Highly Tunable Colloidal Perovskite Nanoplatelets through

Variable Cation, Metal, and Halide Composition, *ACS Nano*, 2016, **10**, 7830–7839.

26 S. Sun, D. Yuan, Y. Xu, *et al.*, Ligand-Mediated Synthesis of Shape-Controlled Cesium Lead Halide Perovskite Nanocrystals via Reprecipitation Process at Room Temperature, *ACS Nano*, 2016, **10**, 3648–3657.

27 X. Peng, L. Manna, W. Yang, *et al.*, Shape control of Cd Se nanocrystals, *Nature*, 2000, **404**, 59.

28 A. Dey, P. Rathod and D. Kabra, Role of Localized States in Photoluminescence Dynamics of High Optical Gain CsPbBr$_3$ Nanocrystals, *Adv. Opt. Mater.*, 2018, **6**, 201800109.

29 Y. Cai, H. Wang, Y. Li, *et al.*, Trimethylsilyl Iodine-Mediated Synthesis of Highly Bright Red Emitting CsPbI$_3$ Perovskite Quantum Dots with Significantly Improved Stability, *Chem. Mater.*, 2019, **31**, 881–889.

30 Y. Li, K. Lu, X. Ling, J. Yuan, G. Shi, G. Ding, J. Sun, S. Shi, X. Gong and W. Ma, High performance planar-heterojunction perovskite solar cells using amino-based fulleropyrrolidine as the electron transporting material, *J. Phys. Chem. A*, 2016, **4**, 10130–10134.

31 C. Sun, Y. Zhang, C. Ruan, *et al.*, Efficient and Stable White LEDs with Silica-Coated Inorganic Perovskite Quantum Dots, *Adv. Mater.*, 2016, **28**, 10088–10094.

32 M. J. Carnie, C. Charbonneau, M. L. Davies, J. Troughton, T. M. Watson, K. Wojciechowski, H. Snaith and D. A. Worsley, A one-step low temperature processing route for organolead halide perovskite solar cells, *Chem. Commun.*, 2013, **49**, 7893–7895.

33 J. Zhu, X. Yang, Y. Zhu, *et al.*, Room-Temperature Synthesis of Mn-Doped Cesium Lead Halide Quantum Dots with High Mn Substitution Ratio, *J. Phys. Chem. Lett.*, 2017, **8**, 4167–4171.

34 Y. Li, L. Dong, N. Chen, *et al.*, Room-Temperature Synthesis of Two-Dimensional Hexagonal Boron Nitride Nanosheet-Stabilized CsPbBr$_3$ Perovskite Quantum Dots, *ACS Appl. Mater. Interfaces*, 2019, **11**, 8242–8249.

35 H. S Anizenlli, R. V. Fernandes, J. Scarmínio, P. R. C. Silva, J. L. Duarte and E. Laureto, Effect of pressure on the remixing process in CH$_3$NH$_3$Pb(I$_{1-x}$Br$_x$)$_3$ perovskite thin films, *J. Lumin.*, 2018, **199**, 348–351.

36 Q. Han, W. Wu, W. Liu and Q. Yang, Two-photon absorption and upconversion luminescence of colloidal CsPbX$_3$ quantum dots, *Opt. Mater.*, 2018, **75**, 880–886.

37 K. J. Lu, J. Zou and T. S. Chung, Novel PVDF membranes comprising n-butylamine functionalized graphene oxide for direct contact membrane distillation, *J. Membr. Sci.*, 2017, **539**, 34–42.

38 E. K. Oikonomou, S. Karpati and S. Gassara, Localization of antifouling surface additives in the pore structure of hollow fiber PVDF membranes, *J. Membr. Sci.*, 2017, **538**, 77–85.

39 C. R. Kagan, E. Lifshitz and E. H. Sargent, Building devices from colloidal quantum dots, *Science*, 2016, **353**, 885.

40 Y. Tao and M. Y. Zou, A General Solvent Selection Strategy for Solution Processed Quantum Dots Targeting High Performance Light-Emitting Diode, *Adv. Funct. Mater.*, 2017, **28**, 1223.